Journal of Alloys and Compounds 509 (2011) 800–804

Contents lists available at ScienceDirect

Journal of Alloys and Compounds

journal homepage: www.elsevier.com/locate/jallcom

Cathodoluminescence of Ce-doped Gd_2SiO_5 and $Gd_{9.33}(SiO_4)_6O_2$ phosphor under continuous electron irradiation

Hiroshi Yokota[a,d,*], Masato Yoshida[a], Hiroyuki Ishibashi[a], Toyohiko Yano[b], Hajime Yamamoto[c], Shinichi Kikkawa[d]

[a] Tsukuba Research Laboratory, Hitachi Chemical Co., Ltd., 48, Wadai, Tsukuba, Ibaraki 300-4247, Japan
[b] Research Laboratory for Nuclear Reactors, Tokyo Institute of Technology, 2-12-1, O-okayama, Meguro-ku, Tokyo 152-8550, Japan
[c] School of Bionics, Tokyo University of Technology, 1404-1, Katakura, Hachioji, Tokyo 192-0982, Japan
[d] Graduate School of Engineering, Hokkaido University, N13W8, Kita-ku, Sapporo 060-8628, Japan

ARTICLE INFO

Article history:
Received 8 June 2010
Received in revised form 9 September 2010
Accepted 17 September 2010
Available online 25 September 2010

Keywords:
Phosphors
Precipitation
Crystal structure
Luminescence

ABSTRACT

Cathodoluminescence was studied on well crystallized Ce-doped Gd_2SiO_5 (GSO:Ce) and $Gd_{9.33}(SiO_4)_6O_2$ (GSAP:Ce) prepared by calcining the hydrolyzed alkoxides at 1573 K because GSO:Ce is easily contaminated with GSAP:Ce impurity in solid state reaction. The luminescence efficiency of GSO:Ce was much higher than that of GSAP:Ce, and Stokes shift of the former was smaller than that of the latter, due to the crystal structural difference between the compounds in Gd_2O_3 and SiO_2 binary chemical composition. The luminescence of GSO:Ce degraded much less than that of GSAP:Ce under the continuous electron irradiation (CL degradation). The CL degradation was related to the formation of the carbon overlayer on the phosphor particles from the vacuum ambient during the irradiation in the present manuscript. The amount of the deposited carbon was influenced by the luminescence efficiency.

1. Introduction

Oxide phosphor materials have attracted attention in the new applications such as plasma display panels (PDPs) and white light emitting diodes (wLEDs) because of the high stabilities [1,2]. The field emission displays (FEDs) application also requires phosphors to have the high stability during continuous electron beam irradiation [3]. Many works on the degradation mechanism under the continuous electron beam irradiation (CL degradation) have been reported on sulfide and oxide phosphor materials [4–12].

Recently, much attention has been focused on oxide phosphors because of the higher stability. Coetsee et al. reported the CL degradation of Ce-doped Y_2SiO_5 (YSO:Ce) particles under the continuous electron beam irradiation with high current density at 10^{-5} Pa oxygen pressure [9–11]. X-ray photoelectron spectroscopy (XPS) showed the formation of silicon dioxide, CeO_2 and CeH_3 layer responsible for the CL degradation. Kim et al. reported that Pr-doped $SrTiO_3$ (STO:Pr) particles degrade even under the low current density electron irradiation at the total vacuum level of 10^{-6} Pa [12]. Auger electron spectroscopy (AES) showed that the carbon overlayer was formed on the phosphor surface during the electron beam irradiation. Carbon species must be derived from the vacuum ambient of the apparatus. The excitation energy of electron is partly wasted in excitation of the crystal lattice vibration to form the new surface layer or to deposit carbon on the crystal surface from the residual organic vapor in the vacuum. However, there have been no studies concerning the degradation properties related to the crystal structure of phosphor materials, to the best of our knowledge.

The silicates of rare earth such as YSO and GSO have been widely investigated for the optical applications, because of the inherent stabilities [13–23]. GSO:Ce has been especially used as the single crystal scintillator having high resistance against the radiation [14,15]. Consequently, GSO:Ce is also expected as the phosphor having high stability against electron beam irradiation, because the mechanism of the cathodoluminescence is almost the same as that of the scintillation. Although synthesis and photoluminescence properties have been reported on GSO polycrystalline phosphor [16–19], there have been no studies about the CL degradation. The growth of the single crystal of GSAP:Ce having similar chemical composition to GSO:Ce has also been reported for the scintillator application [20]. Synthesis and luminescence properties have also been reported on GSAP polycrystalline phosphors [21]. However, there have also been no studies about the CL degradation. Polycrystalline GSO is easily contaminated with GSAP impurity because they are neighboring compounds in Gd_2O_3–SiO_2 binary phase diagram. The GSAP:Ce impurity may affect the CL degradation of GSO:Ce.

* Corresponding author at: Tsukuba Research Laboratory, Hitachi Chemical Co., Ltd., 48, Wadai, Tsukuba, Ibaraki 300-4247, Japan. Tel.: +81 29 864 4399; fax: +81 29 877 1306.
E-mail address: hiro-yokota@hitachi-chem.co.jp (H. Yokota).

0925-8388/$ – see front matter © 2010 Elsevier B.V. All rights reserved.
doi:10.1016/j.jallcom.2010.09.094

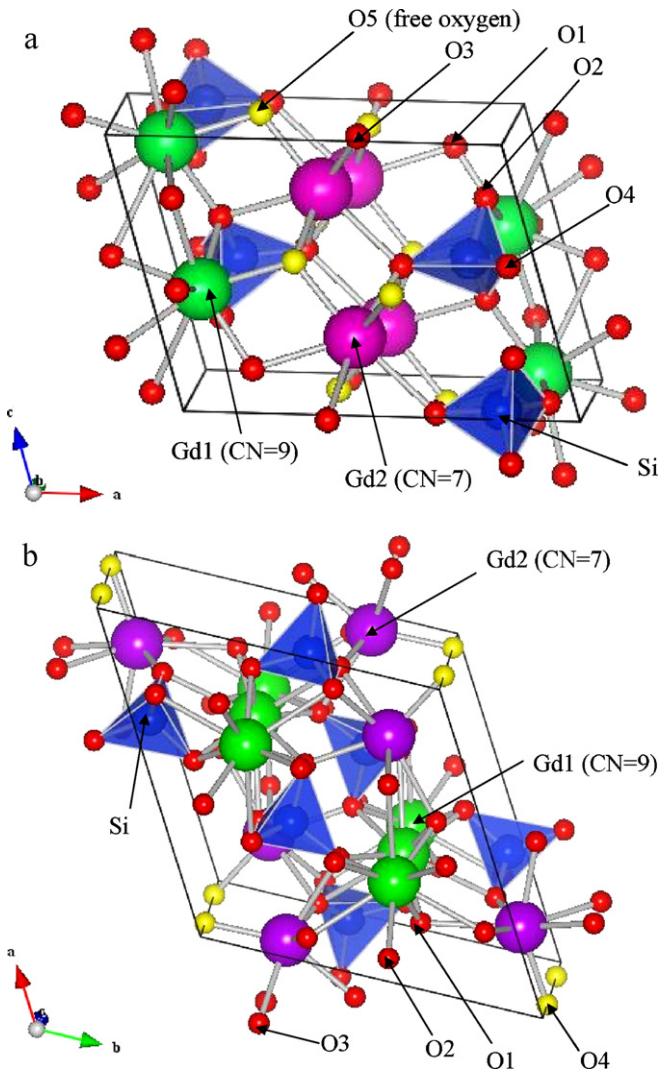

Fig. 1. Schematic drawings of unit cell for (a) Gd_2SiO_5 and (b) $Gd_{9.33}(SiO_4)_6O_2$.

GSO has a monoclinic lattice with the space group $P2_1/c$ (No. 14) [24]. As shown in Fig. 1a, the crystal structure consists of isolated (SiO_4) tetrahedra, free oxygens, and two crystallographically independent Gd atoms (Gd1 and Gd2). The Gd1 site has a coordination number (CN) of 9, with eight oxygens bonded to silicon and one free oxygen. The Gd2 site has a CN of 7, with four oxygens bonded to silicon and three free oxygens. Both sites are in C_1 symmetry. GSAP has a hexagonal lattice with the space group $P6_3/m$ (No. 176) [24]. There are also two kinds of sites, Gd1 (CN = 9) and Gd2 (CN = 7). Gd1 sites have C_3 symmetry, with all oxygens bonded to silicon. Gd2 sites have C_s symmetry, with six oxygens bonded to silicon and one free oxygen (Fig. 1b).

In this research, the polycrystalline phosphor particles of GSO:Ce and GSAP:Ce were prepared by the hydrolysis of alkoxide, and their crystal structure was refined by Rietveld method. The luminescence and the CL degradation were studied in relation to the crystal structure.

2. Experimental

The precursors of GSO:Ce and GSAP:Ce were prepared by the hydrolysis of the stoichiometrically mixed solution of $Gd(NO_3)_3$, $Ce(NO_3)_3$ and $Si(OC_2H_5)_4$ (TEOS) in 4% aqueous ammonia. The adding rate of the solution into the ammonia was 0.1 cm^3/s. The amount of the doped Ce was 0.5 at.% of the total rare earth. The reagents were purchased from Wako Chemicals, and the purity was 99.99%. The precipitants were separated from the solution by the centrifugation, and dried at 423 K. The phosphorous particles of GSO:Ce and GSAP:Ce were finally obtained by calcining each precursor at 1573 K under 0.5% H_2/N_2 reductive atmosphere to avoid the oxidation of Ce^{3+} [22].

Powder X-ray diffraction (XRD) was measured by using X-ray diffractometer (Mac Science, MXP18) at 40 kV and 250 mA with monochromatized CuK_α radiation. The data in $2\theta = 10$–110° were collected with the step scan of 0.05° (2θ) and the dwell time of 8 s at 293 K. The sample was mixed with cellulose resin to eliminate the preferred orientation [23]. Powdered Si (NIST 640c) was used as the external standard for the calibration. Lattice constants were refined by the Rietveld refinement program (RIETAN-2000) [25]. The pseudo-Voigt function was adopted as the symmetric profile shape function in the Rietveld refinement.

Photoluminescence (PL), excitation (PLE) spectra, and internal quantum efficiencies were measured with a fluorescence spectrometer (Hitachi, F-4500). Cathodoluminescence (CL) degradation was evaluated by the intensity change under the continuous electron beam irradiation. The condition was 25 kV, 50 μA in the area of 5 mm × 5 mm (200 μA/cm^2 of current density). The test piece for the CL measurement (CL substrate) was mounted in a vacuum chamber of 10^{-6} to 10^{-7} Pa. The CL substrates were prepared by the conventional sedimentation method [26]. The CL intensity was monitored by the Si photodetector in the chamber. The species of the outgas during the electron beam irradiation were monitored by the quadrupole mass spectrometer (ULVAC, BGM-102).

Table 1a
Unit cell parameters and bond distances of GSO:Ce in monoclinic $P2_1/c$ (No. 14). The analysis reliabilities $R_I = 1.8\%$, and the goodness-of-fit indicators $S(R_{wp}/R_e) = 1.6$. They are compared with literature values for Gd_2SiO_5 [22].

	GSO:Ce	Gd_2SiO_5 (Ref. [22])
Unit cell parameters		
a (nm)	0.9121(0)	0.9131(7)
b (nm)	0.7089(0)	0.7045(6)
c (nm)	0.6738(0)	0.6749(5)
β (°)	107.66(0)	107.52(7)
V (nm^3)	0.415(0)	0.414(1)
Main bond distances (10^{-1} nm)		
Gd1-O1	2.52(2)	2.510
Gd1-O1	2.34(2)	2.276
Gd1-O2	2.37(2)	2.343
Gd1-O2	2.41(3)	2.492
Gd1-O2	2.53(2)	2.559
Gd1-O4	2.56(2)	2.415
Gd1-O4	2.81(2)	2.684
Gd1-O4	2.85(2)	2.768
Gd1-O5	2.36(2)	2.355
Gd2-O1	2.44(2)	2.283
Gd2-O3	2.41(2)	2.383
Gd2-O3	2.48(3)	2.502
Gd2-O3	2.57(2)	2.537
Gd2-O5	2.26(2)	2.294
Gd2-O5	2.30(2)	2.303
Gd2-O5	2.36(3)	2.305
Si-O1	1.66(3)	1.670
Si-O2	1.60(3)	1.631
Si-O3	1.60(3)	1.631
Si-O4	1.58(3)	1.598
Average distances (10^{-1} nm)		
Gd1-O	2.545	2.489
Gd2-O	2.404	2.390

3. Results and discussion

3.1. Crystal structure

The GSO:Ce product crystallized as Gd_2SiO_5 (JCPDS # 40-287) with a very small amount of the impurity of $Gd_{9.33}(SiO_4)_6O_2$ (JCPDS # 38-283) from the stoichiometric mixture of rare earth (RE_2O_3) and TEOS (SiO_2) as shown in Fig. 2a. On the contrary, the pure GSAP:Ce product of $Gd_{9.33}(SiO_4)_6O_2$ depicted in Fig. 2b was obtained from the mixture of $RE_2O_3/SiO_2 = 1/1.3$. The difference in compositions between the starting mixtures and that of the obtained products had been attributed to the difference in the isoelectric point in hydrolysis to obtain RE_2O_3 and SiO_2 raw materials [27].

Lattice constants and representative bond distances obtained by Rietveld analysis were summarized in Table 1. The refine-

ments were well converged on the product without cerium. Lattice constants and the most of the Gd–O distances for GSO:Ce and GSAP:Ce were slightly larger than those reported for Gd_2SiO_5 and $Gd_{9.33}(SiO_4)_6O_2$ without cerium [24], owing to the larger ionic radius of doped Ce^{3+} comparing with Gd^{3+}. Both GSO:Ce and GSAP:Ce have two independent gadolinium sites (Gd1 and Gd2) with CN's of 9 and 7, as shown in Fig. 1. The average distances of Gd–O around Gd1 and Gd2 of GSO:Ce are 0.2545 nm and 0.2404 nm, respectively, as summarized in Table 1a. The corresponding values of GSAP:Ce are 0.2560 nm and 0.2426 nm, as shown in Table 1b. The values in GSO:Ce are shorter than those in GSAP:Ce. The Ce ions are more strongly coordinated with oxide ions in GSO:Ce than in GSAP:Ce. The coordination around Ce is important in a relaxation of the absorbed photon energy.

3.2. Luminescence properties

GSO:Ce showed the excitation (EX) and emission maxima (EM) at around 344 nm and 432 nm, respectively, as shown in Fig. 3. GSAP:Ce had EX at 287 nm and EM at 392 nm, and the wavelength was shorter than that of GSO:Ce. The excitation and emission intensity of GSO:Ce were much higher than that of GSAP:Ce. Table 2 summarizes the values of the Stokes shift and the internal quantum efficiency. The Stokes shift was estimated from the energy difference between EX and EM [28]. The internal quantum efficiency of

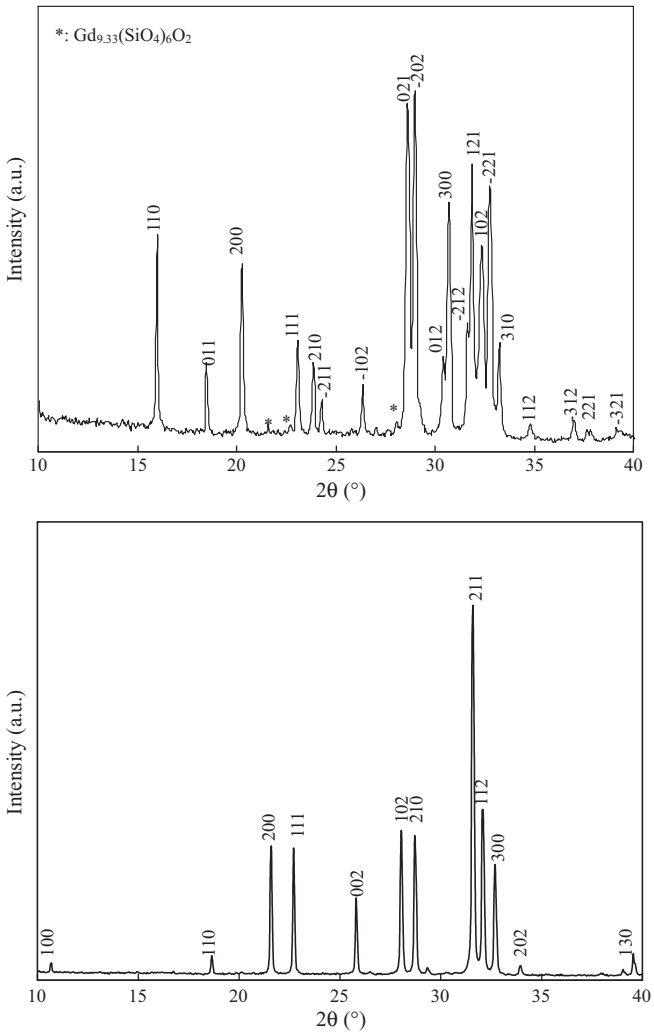

Fig. 2. XRD patterns of (a) GSO:Ce and (b) GSAP:Ce products.

Table 1b
Unit cell parameters and bond distances of GSAP:Ce in hexagonal $P6_3/m$ (No. 176). The analysis reliabilities R_I = 2.4%, and the goodness-of-fit indicators S (R_{wp}/R_e) = 1.5. They are compared with literature values for $Gd_{9.33}(SiO_4)_6O_2$ [22].

	GSAP:Ce	$Gd_{9.33}(SiO_4)_6O_2$ (Ref. [22])
Unit cell parameters		
a (nm)	0.9441(0)	0.9431
c (nm)	0.6861(0)	0.6873
V (nm^3)	0.530(0)	0.529
Main bond distances (10^{-1} nm)		
Gd1-O1	2.408(2)	2.364
Gd1-O1	2.408(2)	2.364
Gd1-O1	2.408(2)	2.364
Gd1-O2	2.486(2)	2.437
Gd1-O2	2.486(2)	2.437
Gd1-O2	2.486(2)	2.437
Gd1-O3	2.787(2)	2.784
Gd1-O3	2.787(2)	2.784
Gd1-O3	2.787(2)	2.784
Gd2-O1	2.625(2)	2.683
Gd2-O2	2.360(2)	2.395
Gd2-O3	2.384(2)	2.294
Gd2-O3	2.384(2)	2.294
Gd2-O3	2.496(2)	2.485
Gd2-O3	2.496(2)	2.485
Gd2-O4	2.235(2)	2.232
Si-O1	1.62(2)	1.620
Si-O2	1.60(2)	1.634
Si-O3	1.66(2)	1.659
Si-O3	1.66(2)	1.659
Average bond distance (10^{-1} nm)		
Gd1-O	2.560	2.528
Gd2-O	2.426	2.410

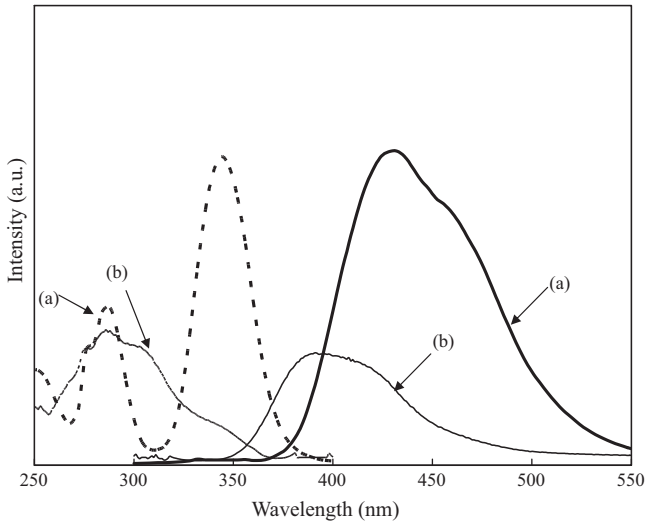

Fig. 3. PL (solid lines) and PLE (doted lines) spectra of (a) GSO:Ce and (b) GSAP:Ce products.

GSO:Ce was much higher than that of GSAP:Ce. And additionally, GSO:Ce had a smaller Stokes shift than GSAP:Ce. These differences can be related to the crystal structural difference, especially the coordination around RE sites. The average Gd–O bond distance was shorter in GSO:Ce than GSAP:Ce as shown in Table 1. The smaller bond distances suggests the crystal field around Ce^{3+} of GSO:Ce is

Table 2
Stokes shift and internal quantum efficiency of GSO:Ce and GSAP:Ce.

	Stokes shift (cm^{-1})	Internal quantum efficiency (%)
GSO:Ce	5922	56.3
GSAP:Ce	9455	11.9

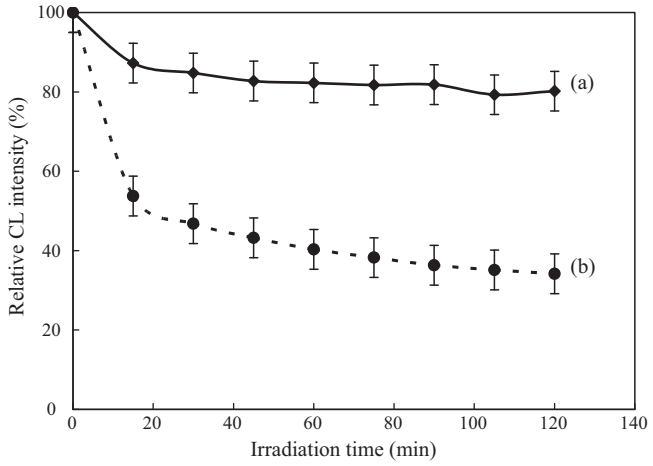

Fig. 4. CL degradation of (a) GSO:Ce and (b) GSAP:Ce products during electron beam irradiation duration.

much stronger than those of GSAP:Ce. The luminescence of Ce^{3+} is caused by the electron transition from 5d to 4f, being affected by the crystal field [29]. Generally speaking, the Stokes shift decreases and the quantum efficiency in luminescence increases with the increasing crystal field strength [28,30].

The CL relative intensity was degraded by the continuous electron beam irradiation. The amount of the degradation of GSO:Ce was much less than that of GSAP:Ce as depicted in Fig. 4. The main species of outgas during the irradiation were H_2, CO and CO_2 as shown in Fig. 5. The amount of outgas was much less in GSO:Ce than GSAP:Ce. It suggests that GSO:Ce was degraded much less than GSAP:Ce in the irradiation depositing less carbon on the surface from organic materials. The surface darkening observed after the irradiation was less significant on GSO:Ce than GSAP:Ce. Kim et al. have reported that the darkening occurred in the irradiation because the carbon overlayer was formed on the phosphor surface under current density of 160 μA/cm^2 electron beam irradiation at the vacuum level of 10^{-6} Pa [12]. Coetsee et al. have reported the formation of the new oxide layer under high current density electron irradiation (26 mA/cm^2) at 10^{-5} Pa oxygen pressure [9–11]. The present electron current density (200 μA/cm^2) and vacuum level (10^{-6} to 10^{-7} Pa) are almost the same as the values in Ref. [12], rather than Refs. [9–11]. So, the reduction of CL intensity observed

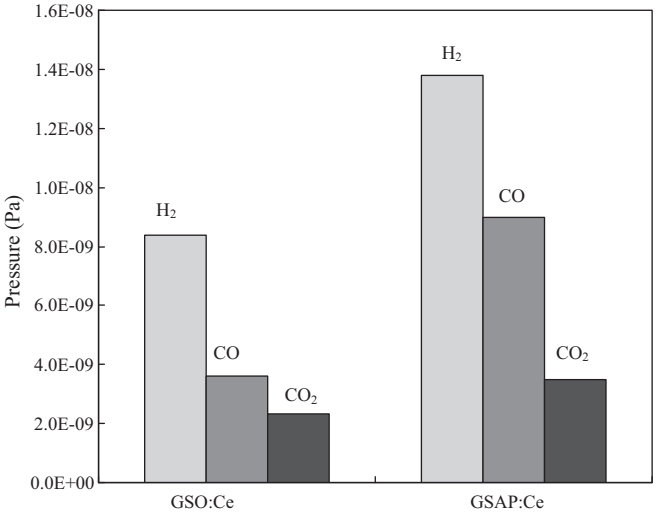

Fig. 5. Outgas species during electron beam irradiation from GSO:Ce and GSAP:Ce products.

Table 3
Calculated heat capacity and temperature of CL substrate for GSO:Ce and GSAP:Ce during electron irradiation.

	Heat capacity (J/mol K)	Heat capacity (J/g K)	Calculated temperature on CL substrate (K)
GSO:Ce	149.9	0.353	544
GSAP:Ce	758.7	0.370	774

in this study may also be related to the carbon overlayer than the oxide layer formed during the irradiation.

The excitation energy of electron is partly wasted in excitation of the crystal lattice vibration [31]. The wasted energy is used to deposit carbon on the crystal surface from the organic vapor in the vacuum. The amount of carbon overlayer on GSO:Ce may be much less than that on GSAP:Ce, depending on the extent of the internal quantum efficiency shown in Table 2. The temperature of CL substrate of GSO:Ce and GSAP:Ce during the irradiation was estimated by using the values of heat capacity and internal quantum efficiency. The heat capacities were calculated as the weighted sum of heat capacities of Gd_2O_3 (105.5 J/mol K) and SiO_2 (44.42 J/mol K) following Neumann-Kopp rule [32]. Assuming that all the energy of electron beam (25 kV/50 μA) is transformed into the cathodoluminescence and the excitation energy of crystal lattice, the calculated heat capacity of GSAP:Ce was higher than that of GSO:Ce per mole but the values in gram are comparable as shown in Table 3. The wasted energy for the lattice excitation was much less in GSO:Ce as discussed in relation to crystal structure above because of the higher internal quantum efficiency shown in Table 2. The substrate temperature was much lower and the deposited carbon amount was much less in GSO:Ce than those in GSAP:Ce, resulting in the larger stability against the CL degradation. GSO:Ce has higher luminescence efficiency because of the more rigid crystal structure than those of GSAP:Ce

4. Conclusions

The cathodoluminescence and the degradation were studied on the phosphor particles of GSO:Ce and GSAP:Ce. The luminescence efficiency was higher, and the Stokes shift was smaller in GSO:Ce than in GSAP:Ce because the coordination distance around Ce is much more shorter. The CL degradation is related to the carbon overlayer formation on the phosphor particles from the vacuum ambient during the irradiation. The CL degradation can be related to the luminescence efficiency on the Ce in the host lattice through the deposited carbon amount under the electron beam irradiation.

Acknowledgement

We thank Mr. H. Aihara, Tokyo University of Technology, for valuable support of CL measurement.

References

[1] W.B. Im, Y.-I. Kim, H.S. Yoo, D.Y. Jeon, Inorg. Chem. 48 (2009) 557–564.
[2] J.H. Lee, Y.J. Kim, Mater. Sci. Eng. B 146 (2008) 99–102.
[3] E.J. Bosze, G.A. Hirata, L.E. Shea-Rohwer, J. McKittrick, J. Lumin. 104 (2003) 47–54.
[4] H.C. Swart, J.S. Sebastian, T.A. Trottier, S.L. Jones, P.H. Holloway, J. Vac. Sci. Technol. A 14 (3) (1996) 1697–1703.
[5] J.S. Sebastian, H.C. Swart, T.A. Trottier, S.L. Jones, P.H. Holloway, J. Vac. Sci. Technol. A 15 (4) (1997) 2349–2353.
[6] H.C. Swart, A.P. Greeff, P.H. Holloway, Appl. Surf. Sci. 140 (1999) 63–69.
[7] H.C. Swart, K.T. Hillie, Surf. Interface Anal. 30 (2000) 383–386.
[8] D.B.M. Klaassen, D.M. de Leeuw, J. Lumin. 37 (1987) 21–28.
[9] E. Coetsee, J.J. Terblans, H.C. Swart, J. Lumin. 126 (2007) 37–42.
[10] H.C. Swart, E. Coetsee, J.J. Terblans, O.M. Ntwaeaborwa, P.D. Nsimama, F.B. Dejene, J.J. Dolo, Appl. Phys. A (2010), doi:10.1007/s00339-010-5915-6.

[11] H.C. Swart, J.J. Terblans, E. Coetsee, V. Kumar, O.M. Ntwaeaborwa, M.S. Dhlamini, J.J. Dolo, Surf. Interface Anal. 42 (2010) 922–926.
[12] J.Y. Kim, Y.C. You, D.Y. Jeon, I. Yu, H.-G. Yang, J. Electrochem. Soc. 149 (2002) H44–H48.
[13] H. Yokota, M. Yoshida, H. Ishibashi, T. Yano, H. Yamamoto, S. Kikkawa, J. Alloys Compd. 495 (2010) 162–166.
[14] T. Kamae, Y. Fukazawa, N. Isobe, M. Kokubun, A. Kubota, S. Osone, T. Takahashi, N. Tsuchida, H. Ishibashi, Nucl. Instrum. Method A 490 (2002) 456–464.
[15] M. Kobayashi, M. Ieiri, K. Kondo, T. Miura, H. Noumi, M. Numajiri, Y. Oki, T. Suzuki, M. Takasaki, K. Tanaka, Y. Yamanoi, M. Ishii, Nucl. Instrum. Method A 330 (1993) 115–120.
[16] B. Yan, H. Huang, Colloids Surf. A: Physicochem. Eng. Aspects 287 (2006) 158–162.
[17] J. Flor, A.M. Pires, M.R. Davolos, M. Jafelicci Jr., J. Alloys Compd. 344 (2002) 323–326.
[18] Y. Wang, B. Chu, Q. He, J. Xu, Appl. Surf. Sci. 254 (2008) 6799–6801.
[19] M.D. Dramicanin, V. Jokanovic, B. Viana, E.A. Fidancev, M. Mitric, Z. Andric, J. Alloys Compd. 424 (2006) 213–217.
[20] Y. Ohgi, H. Kagi, H. Arima, A. Ohta, K. Kamada, A. Yoshikawa, K. Sugiyama, J. Cryst. Growth 311 (2009) 526–529.
[21] T. Hirai, Y. Kondo, J. Phys. Chem. 111 (2007) 168–174.
[22] S.H. Shin, D.Y. Jeon, K.S. Sun, Jpn. J. Appl. Phys. 40 (2001) 4715–4719.
[23] H. Yokota, M. Yoshida, Y. Yagi, H. Ishibashi, T. Yano, H. Yamamoto, Jpn. J. Appl. Phys. 47 (2008) 167–172.
[24] J. Felsche, Structure and Bonding, vol. 13, Springer, Berlin, 1973, pp. 99–197.
[25] F. Izumi, T. Ikeda, Mater. Sci. Forum 321–324 (2000) 198–203.
[26] H. Matsukiyo, T. Suzuki, H. Yamamoto, J. Electrochem. Soc. 143 (1996) 1696–1699.
[27] C.F. Baes Jr., R.E. Mesmer, The Hydrolysis of Cations, Wiley, New York, 1976, pp. 337–342.
[28] J. Lin, Q. Su, H. Zhang, S. Wang, Mater. Res. Bull. 31 (1996) 189–196.
[29] P. Dorenbos, J. Lumin. 99 (2002) 283–299.
[30] J.W.M. Verwey, G. Blasse, Mater. Chem. Phys. 25 (1990) 91–103.
[31] W.M. Yen, S. Shionoya, H. Yamamoto, Fundamentals of Phosphors, CRC Press, New York, 2006, pp. 73–87.
[32] J. Leitner, P. Chuchvalec, D. Sedmidubsky, A. Strejc, P. Abrman, Thermochim. Acta 395 (2003) 27–46.